

---

# Transmission Scanning System for a $\gamma$ Camera Coincidence Scanner

Charles M. Laymon, Timothy G. Turkington, David R. Gilland, and R. Edward Coleman

Department of Radiology, Duke University Medical Center, Durham; and Department of Biomedical Engineering, Duke University, Durham, North Carolina

---

The goal of this research was to develop and evaluate a practical transmission scanning system for attenuation correction on a 2-head  $\gamma$  camera coincidence scanner. **Methods:** The transmission system operates in singles mode and uses point sources of  $^{137}\text{Cs}$  that emit 662-keV  $\gamma$ -radiation. Each point source is inserted between existing septa that are normally used to provide an approximately 2-dimensional emission acquisition geometry. The sources are placed along a line parallel to the axis of rotation near the edge of 1 camera. Data are acquired with the opposing camera. The septa provide axial collimation for the sources so that the transmission system operates in a 2-dimensional offset fanbeam geometry. Camera energy and spatial resolution were measured at 511 and 662 keV. Sensitivity was measured at 662 keV. The effects on axial resolution of adding supplemental collimation to the septa were shown. The system was calibrated and tested using a resolution (rod) phantom and a uniformity phantom. Torso phantom data were acquired. Patient transmission and emission scans were obtained. Postinjection transmission data were used to correct patient emission data. **Results:** The camera resolution at postinjection counting rates was 11.7% full width at half maximum (FWHM) for 662-keV  $\gamma$ -rays. Intrinsic spatial resolution was 2.7 mm (FWHM) at 662 keV. The sensitivity of the system was 280 Hz/MBq using five 74-MBq sources of  $^{137}\text{Cs}$  in the transmission geometry, with supplemental collimation added to the septa to improve axial resolution. The transaxial resolution of the system was such that the smallest rods (6-mm diameter and 12-mm spacing) were well resolved in a reconstructed resolution-phantom image. The corrected patient emission scans were free of attenuation-induced artifacts. **Conclusion:** An easily implemented transmission system for a 2-head  $\gamma$  camera coincidence scanner that can be used for postinjection transmission scanning has been developed.

**Key Words:** attenuation correction;  $\gamma$  camera;  $^{137}\text{Cs}$

**J Nucl Med 2000; 41:692-699**

---

**S**uitably modified rotating  $\gamma$  camera systems operating in a coincidence mode are being used for imaging the distribution of positron-emitting tracers, particularly FDG (1-3). These  $\gamma$  camera coincidence (GCC) systems are a lower cost alternative to coincidence imaging using dedicated PET scanners for some clinical situations.

---

Received Dec. 14, 1998; revision accepted Aug. 9, 1999.  
For correspondence or reprints contact: Charles M. Laymon, PhD, Duke University Medical Center, Box 3949, Durham, NC 27710.

Coincidence emission data are strongly affected by the attenuation produced by the imaging object. However, coincidence emission data can be corrected for attenuation by dividing the counting rate measured along each emission line of response (LOR) by the total attenuation factor (AF) along that line. The attenuation properties of an object and, therefore, the necessary AFs can be deduced experimentally through transmission measurements. Consequently, the ability to perform transmission scans in the GCC modality is desirable, just as it is in dedicated PET.

Some GCC system manufacturers provide transaxial septa for use during coincidence acquisition. Septa limit the axial angular acceptance of the camera, lowering camera counting rates and reducing unusable counts from outside the field of view (FOV). The septa also decrease the counting rate from scattered events as in 2-dimensional PET.

The collimation produced by the septa is useful for a 2-dimensional transmission system as well as for an emission system. We have developed a transmission system for GCC scanners that operates in singles mode using  $^{137}\text{Cs}$  as a source of 662-keV photons (4,5). The system exploits the septa typically used for emission acquisition. The method involves insertion of point radiation sources between the septa of 1 camera. The septa collimate the radiation into transaxial planes as illustrated schematically in Figure 1. The sources are placed along a line (source line), producing an offset fanbeam geometry (6).

A goal of this study was to develop a transmission system that can be installed easily on existing GCC systems. Data from such a system must result in accurate attenuation maps. From a clinical perspective, a transmission system should be able to produce low-noise data for correcting GCC emission data in a small fraction of the time required for a typical emission scan (7). The ability to obtain a postinjection transmission scan is important. This reduces the overall time needed for a complete study and helps to reduce differences in patient position between the transmission and emission scans. A transmission system should also be reliable and easy to use.

This paper describes the transmission system and the results of performance tests. Energy and spatial resolution measurements are presented, as are the results of anthropomorphic phantom and human studies.

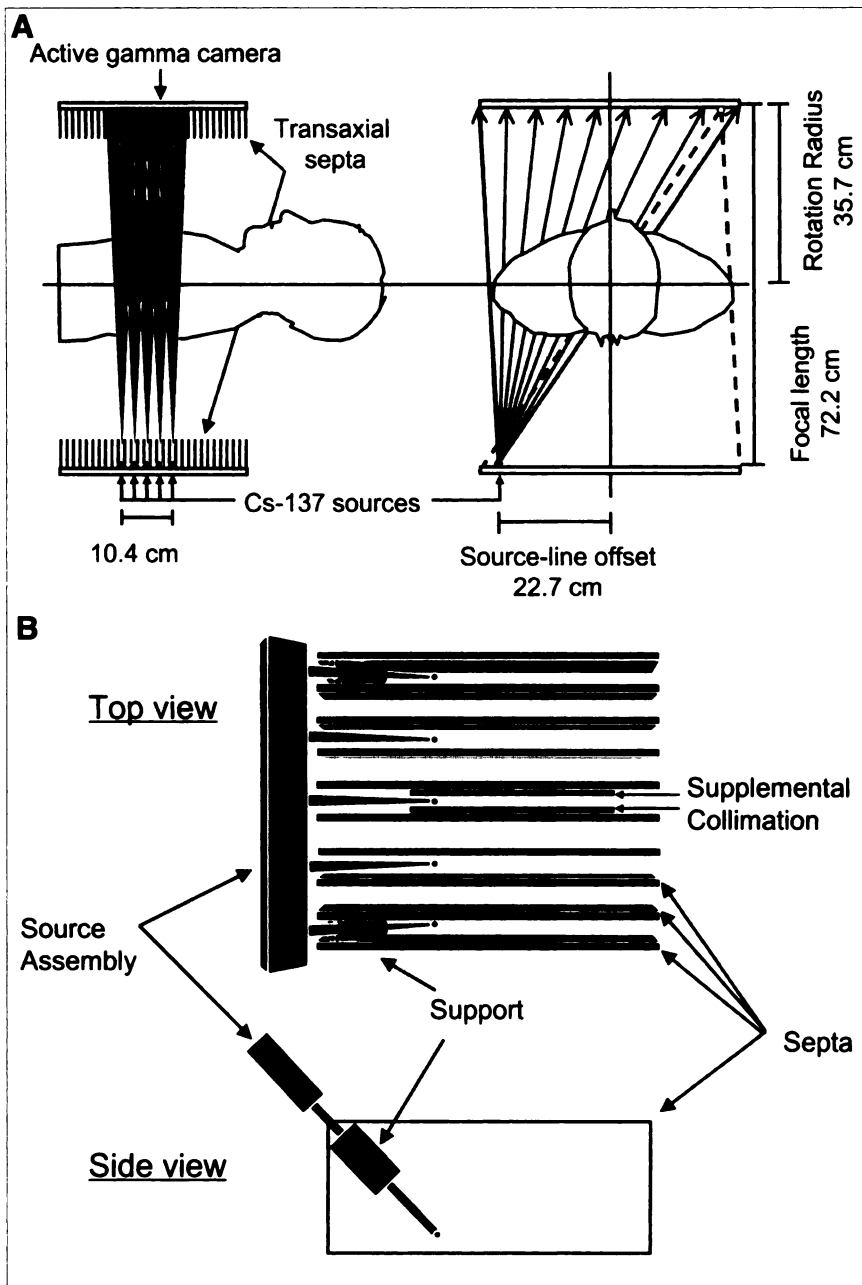


**FIGURE 1.** Transmission system configuration. (A) Schematic view of  $\gamma$  camera with transaxial septa and point sources and resulting radiation field (left) and view along z-axis showing fanbeam geometry (right). Line of sources is mounted on 1 camera. Arrows represent lines of response that are measured with active camera and source camera oriented vertically. Wedge defined by dashed lines indicates sampled region of FOV when cameras are rotated 180°. Lines of response that are missed in 1 camera position are measured in different camera position. (B) Illustration of comblike source assembly mounted on section of camera face.  $^{137}\text{Cs}$  sources are attached to ends of rods. Assembly is inserted at angle to septa. One point source is shown with supplemental collimation. All sources had supplemental collimation in imaging studies.

## MATERIALS AND METHODS

### Scanner

The GCC scanner (Varicam; Elscint, Ltd., Haifa, Israel) used in most of this study was a 2-head  $\gamma$  camera system with an option that allows the camera to run in a high-rate coincidence mode. The scanner was equipped with 1.3-cm (0.5-in.) NaI crystals.

After the initial part of the study, data were acquired using a newer scanner with 1.6-cm (0.625-in.) crystals. The new scanner had improved electronics and software that increased its counting rate capabilities, particularly in singles mode. The improvements allowed patient scanning after injection as well as increased transmission source strength. Energy resolution, sensitivity, and postinjection patient imaging were performed with the upgraded system. As part of the coincidence option for both systems, the

manufacturer supplied transaxial septa in front of graded absorber elements that were used on each camera face (8).

### Transmission System Hardware and Geometry

Transmission data are acquired using an offset fanbeam geometry (6). Definitions and values of the fanbeam parameters are shown in Figure 1. "Point" (1-mm-diameter) sources of  $^{137}\text{Cs}$  (photon energy, 662 keV) are inserted between the septa of 1 camera so that they form a source line parallel to the axis of rotation (z-axis). The camera containing the sources is disabled during a transmission acquisition. For most of the imaging applications reported here, the septa adjacent to each point source were supplemented with additional lead of 1.5-mm thickness to enhance the axial collimation. The additional collimation reduced the slot size from 1.0 to 0.7 cm. Table 1 lists septa and source data relevant

**TABLE 1**  
Transmission System Parameters

System category	Quantity	Value
Septa	Thickness	0.3 cm
	Spacing	1.3 cm
	Depth	6 cm
Sources	Supplemental lead	0.15 (0.3) cm
	Activity/source	74 MBq
	Number used	3 (5)
	Axial spacing	5.2 (2.6) cm
	Axial FOV	13 cm

Values in parentheses were used with upgraded scanner. For upgraded scanner, source depth was decreased from 6 to 3 cm to make room for shielding to protect camera, on which sources were mounted.

to the transmission system. With this geometry, the transmission axial FOV is about 13 cm or about one third the emission FOV.

The  $^{137}\text{Cs}$  point sources are assembled into a single unit, illustrated in Figure 1B, that allows precise positioning and easy mounting and removal. Each transmission source is attached to the end of a thin, 10-cm-long aluminum rod. The other end of each rod is attached to a common acrylic base. The assembly resembles a comb, with the rods as teeth. Two short pieces of plastic tubing, permanently fixed to the septa, serve as supports for the 2 extreme rods of the assembly. The tubes are mounted at the edge of the camera and oriented at an angle to the camera face.

In the studies performed with the original scanner, the sources, when in use, were inserted between the septa until they contacted the graded absorber that forms a base for the septa. In the studies using the new scanner, 3-cm-thick lead shielding was placed at the bottom of the slots underneath each source position to protect the inactive camera from excessive radiation from the transmission sources. This modification was necessary to avoid degradation of that camera's performance after a transmission scan. The shielding decreases the source depth beneath the top of the septa by half. To maintain the same axial collimation of the radiation field, additional lead sheets were used to supplement the septa so that the slots were also reduced to about half the width used in the other imaging studies.

Transmission images were usually acquired with 2.6-cm source spacing. This spacing was accomplished either (before installation of the new scanner) using the 5.2-cm-spaced sources and an interleave operation performed with a 2.6-cm table position shift or (after installation of the new scanner) with a source holder configured with extra sources to achieve actual 2.6-cm spacing.

### System Performance Studies

The basic performance of the system was tested. Measurements required use of the multisource assembly and single  $^{137}\text{Cs}$  sources.

**Energy Resolution.** An important factor affecting the feasibility of postinjection transmission scanning is the energy resolution of the system. To evaluate the separation of 662- and 511-keV photopeaks, we acquired an energy spectrum with the upgraded scanner using a torso phantom that contained approximately 37 MBq FDG. The FDG loading was adjusted to give detector counting rates similar to those seen in patient scans. The total detected event rate from the phantom was 325,000 Hz. This rate includes all events triggering the system event detector. A spectrum

was acquired with the phantom in the FOV and with the source assembly (5 sources spaced at 2.6 cm) in place as for the postinjection patient scan. The source assembly was then removed, and another spectrum was acquired with the phantom still in the FOV.

**Planar Spatial Resolution at 511 and 662 keV.** The spatial resolution of the original  $\gamma$  camera (1.3-cm crystals) was measured at 511 and 662 keV using collimated radiation sources (either a  $^{137}\text{Cs}$  point source or a syringe of FDG). The collimation was formed from 2 lead bricks that were brought into contact along their largest faces, resulting in a submillimeter gap.

For the resolution measurements, no septa or absorbers were used. The camera was covered with a protective plastic window, and the end of the lead brick collimator was placed in contact with the window so that the collimator was approximately 2 cm from the camera face. With this arrangement, the source illuminates a line along the camera face, whose width is much less than the camera resolution. The assembly was positioned so that the projected line was oriented along the x-axis of the camera. Data were acquired with this setup at a series of z-positions separated by 2 cm using both the 511- and the 662-keV sources.

**Sensitivity.** Using the original camera (1.3-cm crystals), sensitivity to 662-keV photons was determined using a 19-MBq point source of  $^{137}\text{Cs}$  placed between the septa of a  $\gamma$  camera so that the point source was positioned along the source line used for transmission acquisition. Data were acquired with the opposite camera using a 20%-wide photopeak energy window. The acquisition was repeated with 1.5-mm-thick sheets of lead inserted on each side of the source and in contact with the septa, as is illustrated schematically in Figure 1. The added lead acted as supplemental collimation and improved axial resolution.

The count rate was also measured using the upgraded camera (1.6-cm crystals). This rate was measured with the transmission source assembly with 5 sources. The sources were configured as for a patient scan, with the sources resting on 3 cm of shielding and with 3 mm of shielding supplementing the septa.

### Imaging Studies

In the studies presented here, attenuation coefficient maps were generated from transmission and blank data by an ordered subset method modified for use with an offset fanbeam geometry (9-12). In all instances, 10 subsets were used in the reconstructions. Detected radiation from the transmission sources was treated in 2 dimensions, as if it originated along the line of sources but in the transaxial plane in which it was detected. Except for the resolution and uniformity studies, data were reconstructed into a  $128 \times 128$  array (pixel size, 0.44 cm).

For each study, blank normalization data were obtained in a 40-min acquisition near the time of acquisition of the transmission data. Blank frames were acquired in  $15^\circ$  steps ( $3^\circ$  steps in the case of the postinjection patient study). The resulting 24 (120) frames were combined to produce a single low-noise normalization frame.

**Transmission Resolution and Uniformity.** To test the resolution and uniformity of the transmission system, 2 phantom studies were performed. The resolution study consisted of a Jaszczak cold rod phantom (Data Spectrum Corp., Hillsborough, NC) inside a 20-cm-diameter, air-filled cylinder. System uniformity was studied using a water-filled 20-cm cylinder.

The reconstruction algorithm requires accurate values for the 3 fanbeam geometry parameters (rotation radius, focal length, and source-line offset), shown in Figure 1, as input. The system

dimensions were measured before the start of the imaging studies. However, to address the issue of uncertainties in the measurements caused by the effects of interaction depth, etc., the data from these studies were also used to fine-tune the geometric parameters used in the reconstruction. Any time changes were made to the system, similar resolution and uniformity studies were performed to determine a revised set of parameters.

The acquisition procedures were the same for the resolution and uniformity measurements. Low-noise transmission data were acquired during a 300-min scan using a 20%-wide photopeak window. The data were placed into 180 projection bins spanning 360°.

For both cases, a 1.8-cm-thick slice at the center of the transmission FOV was reconstructed 100 times using different sets of fanbeam geometry parameters. The trial reconstruction parameters were chosen to bracket the initial physical measurement of the system geometry. For these studies, the reconstruction array size was  $256 \times 256$  (pixel size, 0.22 cm).

**Torso Phantom.** An anthropomorphic torso phantom (Data Spectrum Corp.) was used to investigate image quality achievable with this system as a function of scan duration. The torso was filled with water, and the liver was filled with air. The lungs were filled with water and foam beads, with the result that the attenuation coefficient within the lungs was approximately one third that of water.

A 2.6-cm transmission source spacing was simulated from the existing 5.2-cm spacing by acquiring 2 separate transmission images with the phantom translated by 2.6 cm between scans. The 2 sets of transmission projection data were shifted appropriately and combined. Projection data from the blank scan were duplicated, and the 2 sets were shifted and combined similarly.

These new sets of data (transmission and blank) were smoothed in the axial direction with a boxcar filter with a width equal to the septal spacing. The purpose of this filtering was to eliminate shadows from the active-camera septa. Because the shadow effect is equal in the transmission and blank data, this smoothing procedure primarily makes the noise properties of the image more uniform. The data shifting and application of the filter were simplified because the septal spacing (1.3 cm) was nearly a multiple of the pixel size (0.44 cm).

This procedure was repeated using different acquisition times so that images with different count densities were obtained. In each case, data were reconstructed using 3 iterations of 10 subsets.

**Human Scans.** All human scans were acquired after obtaining informed consent, as required for institutional review board approval. The study participants were patients scheduled to undergo dedicated PET.

A set of patients underwent GCC preinjection transmission studies. Data were acquired into 120 angular bins spanning 360°. Two bed positions were used so that a transmission source spacing of 2.6 cm could be simulated. The acquisition time for each position was 4 min. The transmission data were processed similarly to the torso phantom data. Six iterations were used in the reconstruction. The resulting attenuation maps, measured at 662 keV, were rescaled by a factor of 1.2 to generate maps appropriate for 511 keV. This factor, determined empirically, produced an average soft-tissue attenuation coefficient (0.096/cm, interpolated from narrow-beam values (13)) equal to that of water for 511 keV. The maps were smoothed with a 3-dimensional gaussian filter of 9 mm full width at half maximum (FWHM).

After this portion of the study, the scanner was replaced by the

manufacturer with the updated version with 1.6-cm (0.625-in.) crystals. The new system is being used to perform complete patient studies, including postinjection transmission scans for attenuation correction of emission data.

For the complete study reported here, the patient was injected with 396 MBq (10.7 mCi) FDG 150 min before the start of the GCC imaging studies. The transmission data were acquired similarly to the preinjection data except that the 5-source assembly (2.6-cm spacing) and a single bed position were used with an acquisition time of 4 min.

Immediately before the transmission scan, singles emission data with the patient in place were acquired in a 2-min scan using the transmission configuration and acquisition parameters except that the source assembly was removed from the scanner. These patient background data were used to correct the transmission projection data for 511-keV events that fell into the 662-keV energy window.

After the transmission scan, a GCC emission scan was obtained with the source assembly removed. At the start of the emission acquisition, the total rate in each head was 326,000 Hz (average of the 2 heads), producing a dead time of about 8.3% per head. Two energy windows were used in each camera, a 20% photopeak window and a 94-keV-wide Compton window. Accepted events had at least 1 of the coincident photons registering in the photopeak window, with the other photon registering in either window. Data were acquired in 2° steps (90 bins spanning the 180° coincidence domain) in a 30-min acquisition in which the camera made 10 full rotations.

After subtraction of the background, the transmission data were processed as in preinjection studies except that 4 iterations were used in the reconstruction. The rescaled and smoothed (9-mm FWHM gaussian) attenuation map was projected to match the binning of the emission data. The resulting values represent the integral of the attenuation coefficient along each LOR. These were put into exponential form to produce attenuation correction factors (ACFs).

The emission dataset was smoothed with a 9-mm FWHM gaussian filter. The emission projections were then corrected for attenuation by multiplication with the ACFs. Both the corrected and the uncorrected emission projections were reconstructed by ordered subsets, in which 4 iterations of 10 subsets were used.

Emission, transmission, and background counting rates were compared. A cylindrical surface was defined that fell entirely within the image of the patient, with its axis coincident with the scanner axis of rotation. The cylinder had a diameter of 21.2 cm and a length of 11 slices (4.8 cm) and was near the center of the axial FOV. The numbers of registered counts in the transmission projections, emission projections, and background projections along lines of response that intersected the cylinder were tallied.

## RESULTS

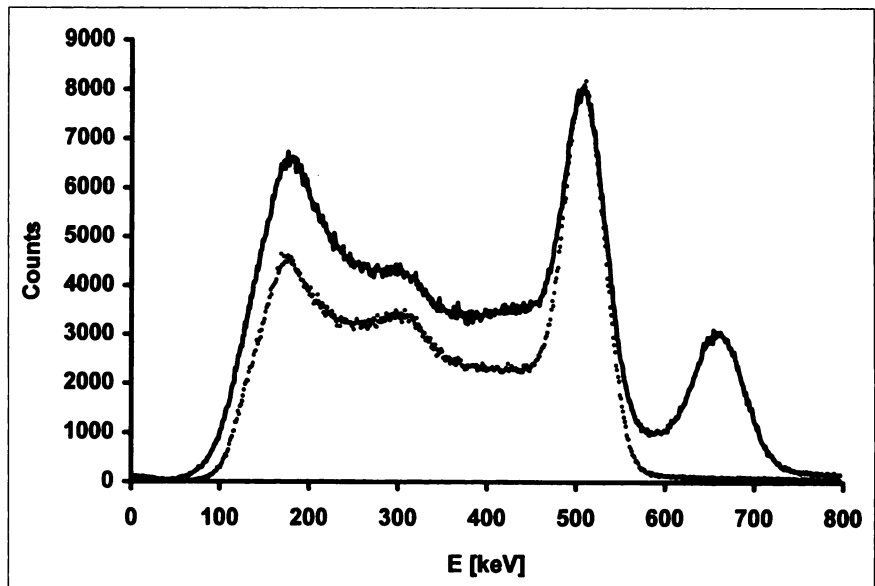
### Energy Resolution

Figure 2 shows the energy spectrum acquired with the torso phantom and the source assembly configured as for a postinjection patient scan.

### Planar Spatial Resolution

The FWHM values averaged over a portion of the camera face for 511 and 662 keV were 2.9 and 2.7 mm, respectively.

**FIGURE 2.** Energy spectra obtained using new scanner (1.6-cm crystals) and torso phantom with activity adjusted to produce counting rate observed in postinjection study. Spectra were taken with 5-source assembly in place (solid curve) and removed (dotted curve). Curves are normalized such that 511-keV photopeaks are same height. Well-resolved 662-keV peak is seen, although it is not completely free of background. Relative sizes of 511- and 662-keV photopeaks are similar to those seen in patient scans. Contamination of  $^{137}\text{Cs}$  photopeak by 511-keV events is small. However, some counts that contribute to  $^{137}\text{Cs}$  photopeak come from photons with trajectories that do not intercept phantom (or patient) and thus are of low value in transmission study. FWHM of  $^{137}\text{Cs}$  photopeak, measured from solid curve, is 11.6%. E = energy.



### Sensitivity

Figure 3 shows the data from the 662-keV sensitivity measurement. Using the original scanner with the 19-MBq source and 1.5 cm of supplemental collimation and a 20% cesium photopeak window, the overall camera sensitivity was 260 Hz/MBq. With the new scanner and the 5-source assembly (total activity, 370 MBq) configured as for a postinjection patient scan, the overall camera sensitivity was 280 Hz/MBq.

### Resolution and Uniformity

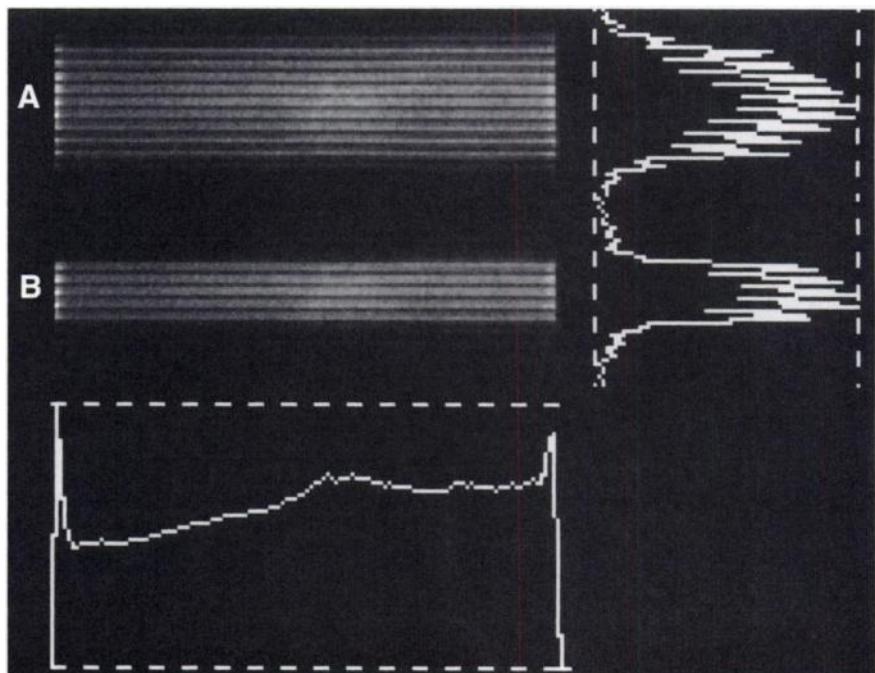
Figure 4 shows the rod and uniformity phantom images judged to be the best of all the trial reconstructions (using different sets of fanbeam parameters) on the basis of image

uniformity, resolution, and the accuracy of the image size compared with the actual object size. The average value of the 662-keV attenuation coefficient deduced from these data is 0.076/cm. This value can be compared with the 0.086/cm interpolated from reference values (13). This difference results, in part, from the detection of scattered events. The geometric parameters used in this reconstruction were also used for subsequent reconstruction and are given in Figure 1. As expected, the adopted parameters were close to the physically measured values.

### Torso Phantom

Figure 5 displays attenuation-coefficient maps resulting from the torso phantom transmission scan.

**FIGURE 3.** Planar images (blank frames) of single point source without (A) and with (B) supplemental collimation. Source position was near right side of image. Next to each image is vertical profile of center of image. Horizontal shadows were produced by septa on active camera. Bottom frame is horizontal profile of B. Axial width of profile is 8 cm and is positioned to include entire bright region of image. Falling image intensity as function of horizontal position is caused by increasing distance between source and camera element in this geometry.



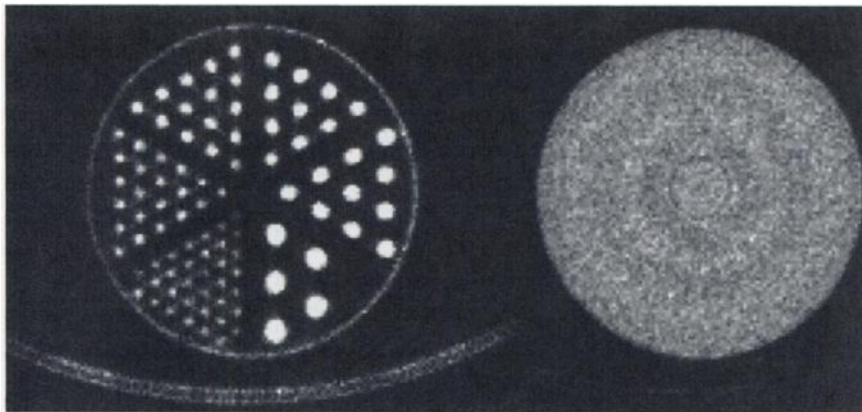


**FIGURE 4.** Rod and uniform-phantom images. Smallest rod diameters are 6 mm, with spacing of 12 mm, and are well resolved. Phantom image is reasonably uniform, although some small ringlike artifacts are visible, indicating slight difference in camera uniformity between blank and transmission scans.

### Human Studies

The results from 5 patient scans acquired without the presence of emission activity are shown in Figure 6.

Transaxial and coronal views of a complete patient scan are presented in Figure 7. The counting rates observed using the cylindrical surface defined in Materials and Methods are summarized in Table 2.

### DISCUSSION

The transmission system described here was easily implemented using the existing transaxial septa normally used for 2-dimensional coincidence emission acquisition. The fan-beam geometry and septa allow a particularly simple transmission source design. Although requiring manual

insertion and removal of the sources, the system is easy to use and reliable because it has no additional moving parts. The expenses associated with installing the system are low, consisting mainly of the cost of purchasing the  $^{137}\text{Cs}$ , a reactor waste product. Furthermore, this isotope has a 30-y half-life and will not need replacement during the service life of the scanner.

Use of  $^{137}\text{Cs}$  as a transmission source has several operational advantages (4,5). The singles mode allows data to be acquired at a much higher rate than does the coincidence mode (14). In singles mode, all detected events in the energy window are used. The coincidence operation on typically available GCC systems does not match most single events with an event in the opposite camera. Additionally, with the energy resolution of NaI(Tl), good separation between 511-

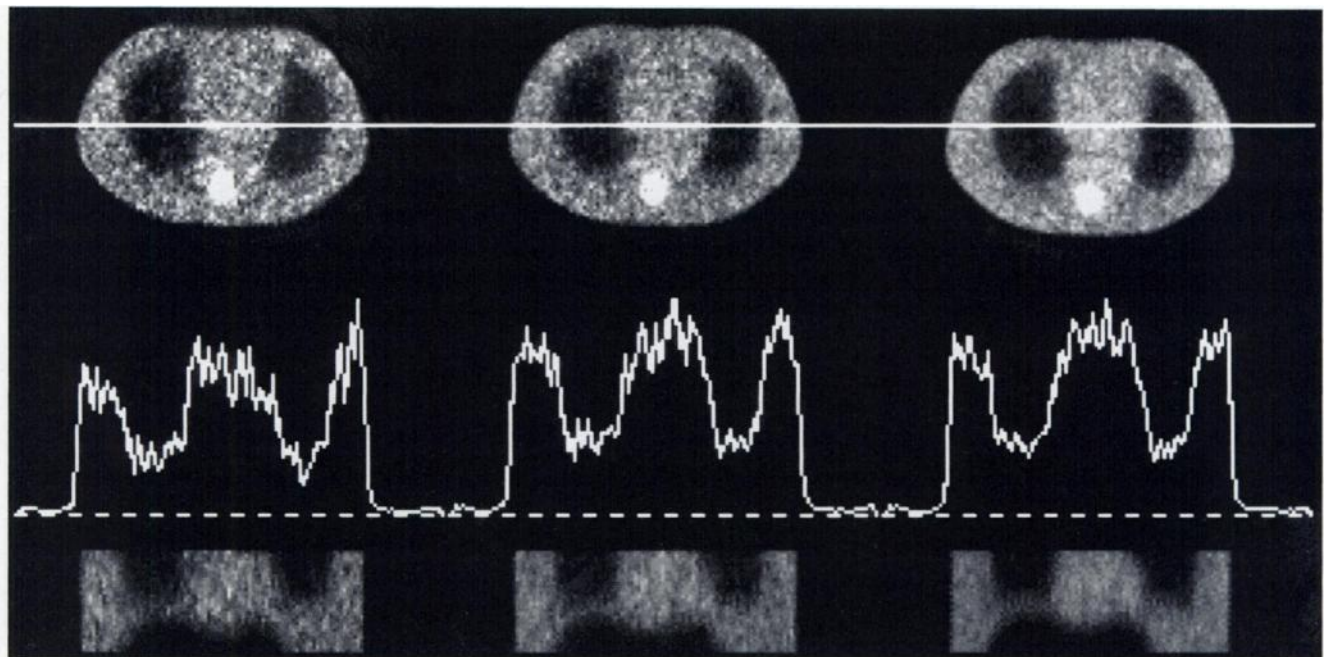
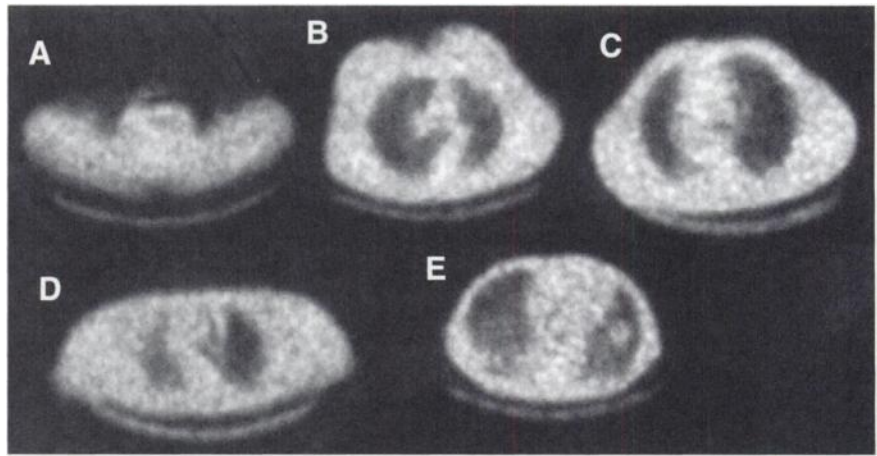


**FIGURE 5.** Torso phantom transaxial (top) and coronal (bottom) images obtained from reconstructed data acquired with 2 bed positions to simulate source spacing of 2.6 cm for scan durations of 3, 6, and 15 min (left to right) per bed position. Profiles were taken along lines shown in transaxial views. Some idea of axial resolution of system (with supplemental collimation and source spacing of 2.6 cm) can be gained from coronal views. Boundary between liver and lung can be differentiated. In phantom, these organs were separated by approximately 1 cm.

**FIGURE 6.** Patient studies. (A–E) Attenuation maps for 5 patients from transmission data acquired without emission activity. Slices shown are at level of neck and shoulders (A) and chest (B–E). Patients' sex, weight, and height were male, 74.4 kg, 180.3 cm (A); female, 82.6 kg, 154.9 cm (B); male, 92.5 kg, 185.4 cm (C); male, 66.2 kg, 172.7 cm (D); and male, 58.1 kg, 172.1 cm (E). At shoulder level, attenuation is nonisotropic with large values along LORs that pass through both shoulders. Chest-level images include lungs, and (E) shows large mass in left lung (right side of image).



and 662-keV photopeaks is possible, as shown in Figure 2, allowing postinjection transmission scans.

Axial resolution is an important design consideration. To address this issue, one must have a good understanding of the axial resolution requirements of a transmission system, given the emission image properties with which the transmission data will be used and the local translational symmetries within the body. We have begun a study to address this topic.

The axial resolution of the system itself is a complicated topic and is being addressed in a separate project. In some tests, a set of 1.3-cm-wide acrylic disks were placed in the FOV such that their flat sides were perpendicular to the rotation axis. Disks were well resolved when their spacing (periodicity) was 4.3 cm (15).

The transmission axial resolution is determined mainly by the axial angular divergence of the radiation field emitted by the sources. The divergence can be controlled well by adjusting the axial collimation (Fig. 3). As illustrated schematically in Figure 1, one can adjust this collimation by

supplementing the septa with small sheets of lead (or other dense material). Using various amounts of supplemental shielding, one can produce almost arbitrary radiation field collimation.

An issue closely related to axial resolution is sampling. Too small a source density results in undersampled regions. The minimum source density is therefore determined by the axial divergence defined by the axial collimation. Source density can be increased by adding more sources. Additionally, an arbitrary effective source density can be achieved by scanning with different bed positions. Thus, the system is flexible in that its axial properties can be modified, if necessary, to meet more stringent requirements.

The current transmission system has an axial FOV of 13 cm, or approximately one third the emission FOV. A planned modification to the system will extend the transmission FOV by adding sources.

Another avenue for improving the capabilities of the system is data processing. We are investigating the use of

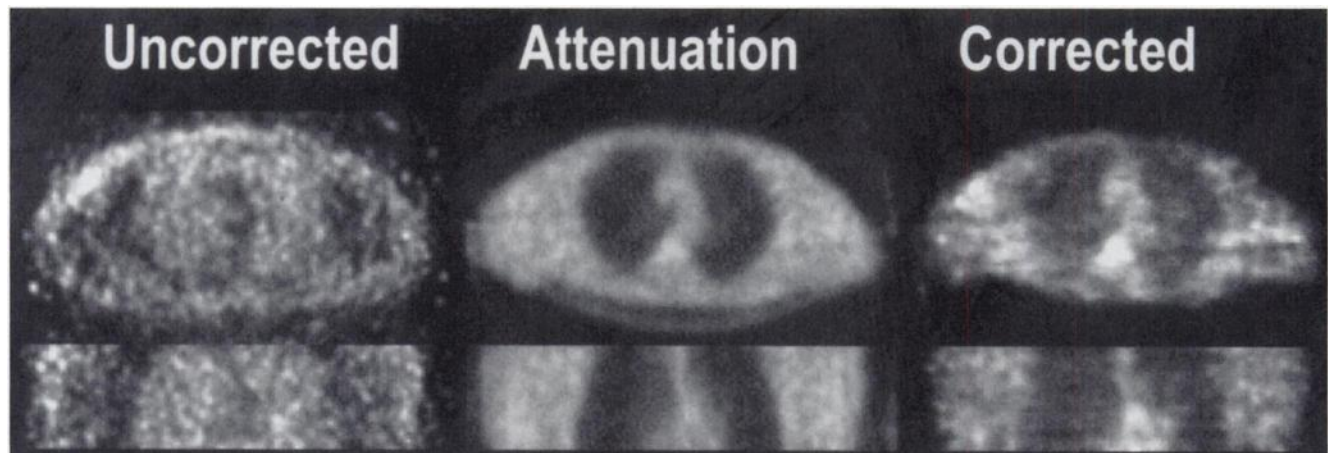


**FIGURE 7.** Study of male patient (weight, 73.9 kg; height, 175.3 cm) shows transaxial (top row) and coronal (bottom row) views of uncorrected emission image, attenuation map from postinjection transmission data, and corrected emission image. Attenuation correction produced expected effect on emission maps. In particular, lungs appear dark on corrected images and bright on uncorrected images, and lung boundaries are clearer on corrected images. Bright rim (attenuation artifact) around part of outer body contour on uncorrected image is absent on corrected image. No significant structural or metabolic abnormalities were observed in these images or in dedicated PET study for this patient.

**TABLE 2**  
Count Rates Observed over Portion of FOV  
During Patient Scan

Scan type	Duration (s)	Counts	
		intercepting cylinder	Rate (cps)
Transmission	240	770,000	3,200
Emission background (singles)	120	35,000	300
Emission (coincidence)	1,800	590,000	330

transmission image segmentation to reduce noise and to ameliorate inaccuracies associated with scatter and possible contamination from 511-keV photons (16,17).

## CONCLUSION

We have developed a transmission scan system for a GCC scanner. The system was easily implemented using point sources of  $^{137}\text{Cs}$  in an offset fanbeam geometry and minor modifications to transaxial septa commonly used for emission acquisition. The system has been used to obtain a postinjection transmission scan. The data were used to correct a coincidence emission scan for attenuation.

## ACKNOWLEDGMENTS

The authors thank Sharon M. Hamblen and Eddie Wheeler for data acquisition and Dr. Michael W. Hanson for helpful comments. This work was supported by Elgems, Ltd., Haifa, Israel, and in part by the National Institutes of Health, through grant R29 HL52162, and The Whitaker Foundation.

## REFERENCES

- Jarritt PH, Acton PD. PET imaging using gamma camera systems: a review. *Nucl Med Commun.* 1996;17:758-766.
- Smith EM, O'Mara RE. 511 keV imaging: SPECT, coincidence, or both? *Appl Radiology.* 1996;25:6-27.
- Coleman RE, Laymon CM, Turkington TG. FDG imaging of lung nodules: a phantom study comparing SPECT, camera-based PET, and dedicated PET. *Radiology.* 1999;210:823-828.
- Karp JS, Muehllehner G, Qu H, Yan X-H. Singles transmission in volume-imaging PET with a  $^{137}\text{Cs}$  source. *Phys Med Biol.* 1995;40:929-944.
- Yu SK, Nahmias C. Single photon transmission measurements in positron tomography using Cs-137. *Phys Med Biol.* 1995;40:1255-1266.
- Chang W, Loncaric S, Huang G, Sanpitak P. Asymmetric fan transmission CT on SPECT systems. *Phys Med Biol.* 1995;40:913-928.
- Laymon CM, Turkington TG, Coleman RE. Attenuation effects in gamma-camera coincidence imaging. *IEEE Trans Nucl Sci.* 1998;45:3115-3121.
- Muehllehner G, Jaszczak RJ, Beck RN. The reduction of coincidence loss in radionuclide imaging cameras through the use of composite filters. *Phys Med Biol.* 1974;19:504-510.
- Hudson HM, Larkin RS. Accelerated image reconstruction using ordered subsets of projection data. *J Nucl Med.* 1994;39:601-609.
- Lange K, Carson R. EM reconstruction algorithms for emission and transmission tomography. *J Comput Assist Tomogr.* 1984;8:306-316.
- Siddon RL. Fast calculation of the exact radiological path for a three-dimensional CT array. *Med Phys.* 1985;12:252-255.
- Gilland DR, Jaszczak RJ, Greer KL, Coleman RE. Transmission imaging for nonuniform attenuation correction using a three-headed SPECT camera. *J Nucl Med.* 1998;39:1105-1110.
- Hubbell JH. Photon cross-sections, attenuation coefficients, and energy absorption coefficients from 10 keV to 100 GeV. *Natl Stand Ref Data Ser.* 1969;29:62-66.
- deKemp RA, Nahmias C. Attenuation correction in PET using single photon transmission measurement. *Med Phys.* 1994;21:771-778.
- Turkington TG, Laymon CM, Schopfer KG, Coleman RE, Wainer N. Multiple point sources collimated with transaxial septa for high energy gamma camera transmission scanning. *IEEE Trans Nucl Sci.* 1999;46:2247-2252.
- Xu EZ, Mullan NA, Gould KL, Anderson WL. A segmented attenuation correction for PET. *J Nucl Med.* 1991;32:161-165.
- Meckle SR, Dahlbom M, Cherry SR. Attenuation correction using count-limited transmission data in positron emission tomography. *J Nucl Med.* 1993;34:143-150.